Light Emission Characteristics and Mechanics of Foldable Inorganic Light-Emitting Diodes

By *Sang-Il Park, An-Phong Le, Jian Wu, Yonggang Huang, Xiuling Li,* and *John A. Rogers**

Organic light emitting diodes (OLEDs) offer attractive alternatives to conventional inorganic devices due to their ability to be deposited over large areas on amorphous, thin flexible substrates, for systems with lightweight, durable, and compact designs.[1,2] Recent work suggests that inorganic light-emitting diode (ILED) technologies can be adapted to reproduce many of these characteristics,[3] while at the same time providing performance advantages in brightness, robust operation and efficiency.[3–5] Here we report advances in this type of ILED approach designed to enable degrees of bendability than significantly exceed those previously achieved,[3] by exploiting concepts of neutral mechanical plane designs that we successfully developed for use in other flexible inorganic device technologies in electronics[6] and photovoltaics.[7] The studies include quantitative analysis of the underlying mechanics, with the first direct connections between such calculations and device performance through experimental measurements of bending induced shifts in the emission wavelength. The results provide strategies to achieve bending to radii as small as 0.7 mm with negligible changes in the electrical properties or the emission wavelengths (to within less than ~1 nm) of the devices. This outcome exceeds even the best levels of bendability in literature reports of OLEDs where bending radii as small as several millimeters have been achieved.[8–11] Such devices might be useful for applications that require mechanical properties that are normally associated with OLEDs but with the performance offered by ILEDs.

Figure 1 schematically illustrates the key processing steps for fabricating the devices. Etching and release strategies first define microscale ILEDs from specialized epitaxial semiconductor layers grown on top of a sacrificial layer ($Al_{0.96}Ga_{0.04}As$) on a GaAs wafer, following procedures reported recently.[3] The stacks consist, specifically, of 5 nm thick p-GaAs (GaAs:C), 800 nm thick p-spreader ($Al_{0.45}Ga_{0.55}As$:C), 200 nm thick p-clad ($In_{0.5}Al_{0.5}P$:Zn), InGaP quantum well structures (6 nm thick $In_{0.56}Ga_{0.44}P$ wells, with 6 nm thick barriers of $Al_{0.25}Ga_{0.25}In_{0.5}P$ on top and bottom), 200 nm thick n-clad ($In_{0.5}Al_{0.5}P$:Si), 800 nm thick n-spreader ($Al_{0.45}Ga_{0.55}As$:Si), and 500 nm thick n-GaAs (GaAs:Si). Techniques of transfer printing[3,6,7,12–14] lift these devices from the wafer and deliver them in sparse arrays onto sheets of polyethylene terepthalate (PET; Grafix DURA-LAR, 50 μm thick) coated with thin layers of a photocurable polyurethane (NOA61, Norland Products Inc., spun at 5000 rpm/60 sec) as an adhesive. Next, wet etching through the top layers (p-GaAs/p-spreader by $H_3PO_4/H_2O_2/H_2O$ (1:13:12), InAlGaP-based layers by HCl/H_2O (2:1), and n-spreader by $H_3PO_4/H_2O_2/H_2O$ (1:13:12)) exposes just the n-GaAs at the base. In this way, contacts to the p and n sides of the device can be formed easily by planar, thin film processing of metal, as shown in Figure 1a. The scanning electron microscope (SEM) image of Figure 1a shows an angled view (45° tilted) of a individual ILED (width × length × thickness = 100 μm × 100 μm × 2.523 μm), partially embedded in the polyurethane layer, after printing and etching. An epoxy coating (SU8-2, Microchem., spun at 1500 rpm/30 sec) prevents electrical shorting through the sidewalls of the ILEDs, and also provides partial planarization of the devices (total thickness ~2.5 μm) as illustrated in Figure 1b. The polymers used here have negligible absorption in the visible range. Figure 1c shows electrodes used to establish electrical connection to the devices, formed by photolithography and etching of metallization (20/350 nm thick Ti/Au) deposited by electron beam evaporation. The optical micrograph of Figure 1c shows a top view. Figure 1d illustrates an encapsulation process that relies on epoxy material patterned to provide openings for electrical probing, and with different thicknesses in different regions. As described subsequently, the choice of thickness of the encapsulation layer is a key design parameter

[*] Prof. J. A. Rogers
Department of Materials Science and Engineering
Chemistry, Mechanical Science and Engineering, Electrical and Computer Engineering
Beckman Institute for Advanced Science and Technology and Frederick Seitz Materials Research Laboratory
University of Illinois at Urbana-Champaign
Urbana, Illinois 61801 (USA)
E-mail: jrogers@illinois.edu
S.-I. Park
Department of Materials Science and Engineering
Beckman Institute for Advanced Science and Technology and Frederick Seitz Materials Research Laboratory
University of Illinois at Urbana-Champaign
Urbana, Illinois 61801 (USA)
A.-P. Le
Department of Chemistry
Beckman Institute for Advanced Science and Technology and Frederick Seitz Materials Research Laboratory
University of Illinois at Urbana-Champaign
Urbana, Illinois 61801 (USA)
J. Wu, Prof. Y. Huang
Department of Civil and Environmental Engineering and Mechanical Engineering
Northwestern University
Evanston, IL 60208 (USA)
Prof. X. Li
Department of Electrical and Computer Engineering
University of Illinois at Urbana-Champaign
Urbana, Illinois 61801 (USA)

DOI: 10.1002/adma.201000591

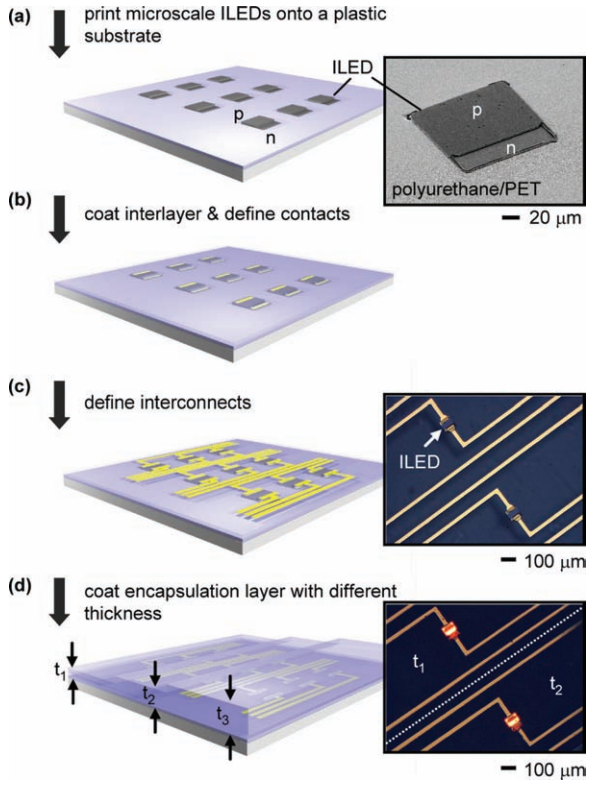

Figure 1. Schematic illustrations (left frames) of processing steps for fabricating bendable ILED systems with encapsulation layers of different thicknesses on a plastic substrate, and representative images (right frames). a) Transfer printing delivers arrays of microscale ILEDs to a PET substrate coated with a polyurethane layer. Etching exposes the bottom, n-GaAs on one edge of each device. The SEM image on the right shows a individual ILED (~2.5 μm thick) partially embedded in the polyurethane layer on the PET substrate. b) Coating and photopatterning a thin layer of epoxy on top of the devices and then depositing ohmic metals forms n and p contacts. c) Photolithographic patterning establishes interconnection lines for electrical probing. d) Coating and photopatterning defines encapsulation layers with different thicknesses in different regions. Optical micrographs of c), d) show top views of interconnected ILEDs in their off and on states, respectively. The top and bottom regions of frame (d) have encapsulation layer thicknesses of t_1 and t_2, respectively.

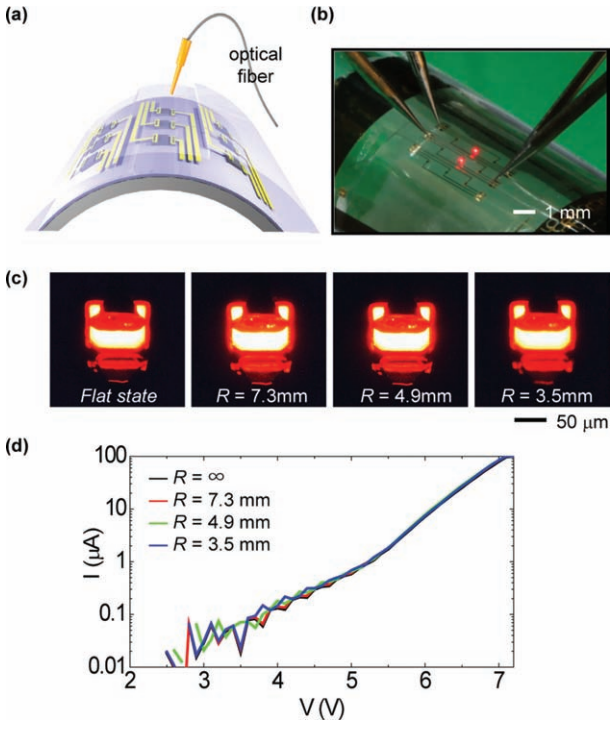

Figure 2. a) Schematic illustration and b) optical image of small, square ILEDs (100 × 100 μm, ~2.5 μm thick) formed on plastic substrate (PET, 50 μm thick) coated with polyurethane layer, in a bent configuration (R ~ 7.3 mm) during operation. c) Optical micrographs of light emission from individual ILEDs at bending radii of ∞, 7.3, 4.9, and 3.5 mm, respectively. d) Current (I) – voltage (V) measurements as a function of bending radius (∞, 7.3, 4.9, and 3.5 mm).

for controlling the bending mechanics. Multiple cycles of spin casting and photopatterning processes establish multiple thicknesses of encapsulation layer on the substrate. This layout leads to different strains in different ILEDs on a single substrate subjected to bending. The optical microscope image in Figure 1d shows emission from ILEDs with different encapsulation layer thicknesses (t_1 and t_2).

We began by characterizing the emission of devices like those in Figure 1 under bending, by use of a high resolution spectrometer (Ocean Optics, HR-4000; ~0.5 nm resolution). **Figure 2**, a and b, show a schematic illustration and an optical image of small, square lighting devices (100 μm × 100 μm) formed on a thin sheet of plastic (PET, 50 μm thick) with a layer of a photocurable polyurethane (~2.5 μm) as an adhesive in a bending state, characterized by a radius of curvature, R, of ~7.3 mm. The optical fiber, as illustrated in Figure 2a, collects emitted light and transports it to the spectrometer. Figure 2c presents optical micrographs of individual ILEDs in operation at bending radii of ∞, 7.3, 4.9, and 3.5 mm, respectively. The optical images show that there is no observable change, even to the smallest bending radius (R ~ 3.5 mm). Current (I, log scale) – voltage (V) characteristics, as a function of bending radius of curvature, support these observations, as shown in Figure 2d.

On the other hand, the emission spectra show small, but systematic, changes with bending, as shown in **Figure 3a** for the case of an encapsulation layer with thickness of ~ 5.5 μm. In particular, as the bending radius decreases to R ~ 3.5 mm, the emission wavelength increases by ~3.8 nm ± 0.2 nm. These shifts were determined simply by recording the wavelength position of the peak in the emission spectra. These changes are attributable to shifts in the bandgap induced by mechanical strains. To explore this behavior in detail, we analyzed the mechanics and then evaluated the bandgap shifts expected based on the computed strains, as described in the following. First, treating this system as a composite beam[3,15] yields the following expression for the distance between the neutral mechanical plane and the top surface

$$h_{neutral} = \sum_{i=1}^{N} \bar{E}_i h_i \left(\sum_{j=1}^{i} h_j - \frac{h_i}{2} \right) \Big/ \sum_{i=1}^{N} \bar{E}_i h_i \qquad (1)$$

where N is the total number of layers, h_i is the thickness of the i^{th} layer (from the top), and is $\bar{E}_i = E_i/(1 - v_i^2)$ is related to the

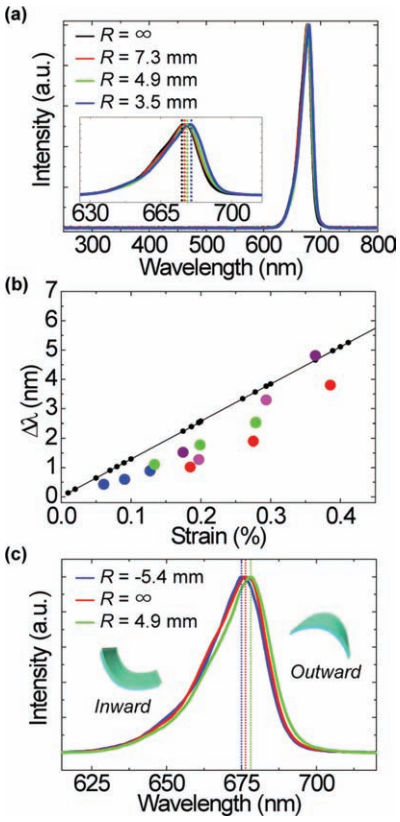

Figure 3. a) Spectral characteristics of emission from ILEDs encapsulated with a ~5.5 μm thick layer of epoxy on a PET substrate (50 μm thick) at bend radii of ~∞, 7.3, 4.9, and 3.5 mm. The inset shows the same data plotted from 625 nm to 715 nm. b) Change in the center wavelength of emission (Δλ) calculated (black) and experimentally measured (various colors) as a function of maximum uniaxial strain in the quantum wells of the ILEDs. c) Emission spectra of an ILED in a flat state ($R \sim \infty$), during inward bending ($R \sim -5.4$ mm), and outward bending ($R \sim 4.9$ mm). The corresponding shifts in the emission wavelength are $\Delta\lambda \sim -1.27$ nm (inward) and $\Delta\lambda \sim 1.77$ nm (outward).

Young's modulus E_i and Poisson's ratio ν_i of the i^{th} layer. The strain in the ILED, including the quantum well, is given by

$$\varepsilon = y/R \tag{2}$$

where R is the bend radius, and y is the distance from the neutral mechanical plane. For the system of Figure 1d, the elastic properties and layer thicknesses are (1) $E_{encapsulation}$ = 4.4 GPa, $\nu_{encapsulation}$ = 0.44, and $h_{encapsulation1}$ = 4.6 μm and $h_{encapsulation2}$ = 0.877 μm for the two encapsulation layers above and below the electrode, respectively; (2) $E_{electrode}$ = 78 GPa, $\nu_{electrode}$ = 0.44, and $h_{electrode}$ = 300 nm; (3) E_{ILED} = 77.5 GPa, ν_{ILED} = 0.312, and h_{ILED} = 2.523 μm; (4) $E_{adhesive}$ = 1 GPa, $\nu_{adhesive}$ = 0.3, and $h_{adhesive}$ = 2.5 μm; and (5) $E_{plastic}$ = 4 GPa, $\nu_{plastic}$ = 0.44 and $h_{plastic}$ = 50 μm. The neutral mechanical plane is 20.2 μm below the top surface. The maximum distance from the quantum well to the neutral mechanical plane is then 13.4 μm, which gives a maximum strain of nearly 0.4% in the quantum well for a bending radius R = 3.5 mm.

The expected strain dependence of the emission wavelength can be evaluated with $k{\cdot}p$ perturbation theory.[3,16–18] The bending deformations correspond to in-plane uniaxial stresses defined along the x direction; stresses in the y and z directions are zero ($\sigma_{yy} = \sigma_{zz} = 0$). The strains in these directions due to the Poisson's effect are given by

$$\varepsilon_{yy} = \varepsilon_{zz} = -\nu\varepsilon_{xx} \tag{3}$$

where the Poisson's ratio ν is related to the elastic stiffness constants C_{11} and C_{12} by $\nu/(1-\nu) = C_{12}/C_{11}$. For the small stress range examined here, the strain induced bandgap shifts for heavy hole (HH) and light hole (LH) are given by

$$\delta Eg^{LH} = \delta E_H + \delta E_S \tag{4}$$

$$\delta Eg^{HH} = \delta E_H - \delta E_S \tag{5}$$

where $\delta E_H = a(\varepsilon_{xx} + \varepsilon_{yy} + \varepsilon_{zz})$, $\delta E_S = (b/2)(\varepsilon_{xx} + \varepsilon_{yy} - 2\varepsilon_{zz})$ and δE_H, and δE_S are the hydrostatic-pressure shift and the uniaxial stress-induced valence-band splitting, respectively,[16–18] and a and b are the corresponding deformation potentials. For the quantum well ($In_{0.56}Ga_{0.44}P$) in the ILED structure studied here, the above parameters are a = –7.42 eV, b = 1.91 eV, C_{11} = 11.936×10^{11} dyne/cm^2, and C_{12} = 5.975×10^{11} dyne/cm^2.[3,19] Assuming HH is the ground state for the quantum well,[19] the uniaxial mechanical stress induced bandgap shift in the ILED is ~4.9 nm, for a maximum bending strain of ε_{xx} = 0.384 %.

Figure 3b shows the calculated emission wavelength shift (black) and experimentally measured shifts (various colors; error bars comparable to symbol sizes) as a function of the calculated maximum uniaxial strain in the quantum well of the ILED. The strains depend both on the bending radii (7.3 mm, 4.9 mm, and 3.5 mm) and the thickness of the encapsulation layer. The calculations show reasonably good agreement with measurement, thereby providing some validation of the underlying physics. Many similar considerations apply to inward bending, which leads to compressive strains in the quantum well. Figure 3c shows the emission spectra in cases of both inward and outward bending. Outward bending leads to increases in the wavelength (red shift, $\Delta\lambda \sim 1.77$ nm) at a bending radius of 4.9 mm. By contrast, inward bending ($R \sim 5.4$ mm) reduces the wavelength (blue shift, $\Delta\lambda \sim -1.27$ nm). The calculated maximum strains in the quantum well of the ILED system in these two cases are 0.275% tensile and 0.250% compressive. Slight discrepancies between experiment and theory can be caused by compositional variations, defects induced by compressive strains during fabrication, or uncertainties in values of parameters (moduli, dimensions or electronic properties) used in the modeling.

Although the magnitudes of the shifts in emission wavelength for the examples shown previously are likely to be unimportant for most applications, strategies that reduce the strains that give rise to these shifts can minimize mechanically induced degradation at interfaces or, ultimately, fracture in the devices. One solution is to configure the layouts to place the ILEDs near the neutral mechanical plane. The position of this plane can be computed by equation (1). **Figure 4a** shows a schematic illustration of a layout that achieves this outcome. The process involves fabrication on a temporary substrate of PET that is peeled away as a final step. Here, the ILEDs are positioned in the middle, with layers of polyurethane on top and bottom. The total thickness

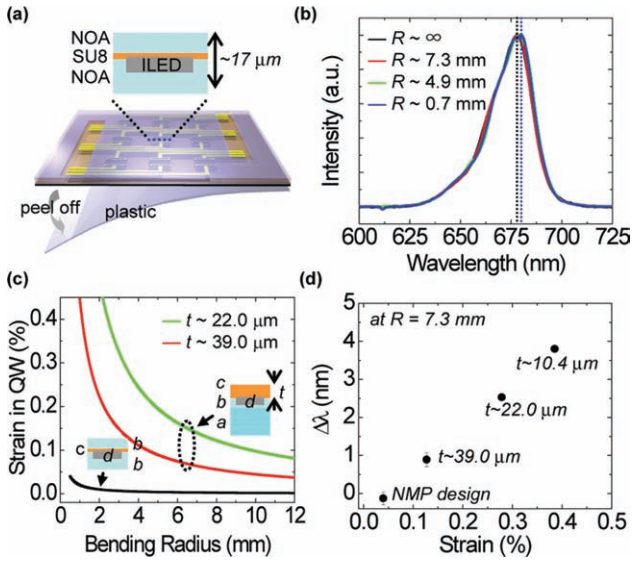

Figure 4. a) Schematic illustration of an ILED system placed near the neutral mechanical plane, and with a total thickness of ~17 μm. Here, PET serves as a temporary substrate that is peeled away as a final step in the fabrication. b) Spectral characteristics of emission of an ILED placed near the neutral mechanical plane, at bending radii of ∞, 7.3, 4.9, and 0.7 mm. The emission wavelength shifts by ~1 nm over this entire range. c) Calculated maximum strain in the quantum wells of ILEDs encapsulated by epoxy (22.0 and 39.0 μm thick) on a PET substrate and in the neutral mechanical configuration of frame (a), as a function of bending radius. d) Shift in the wavelength of emission for ILEDs encapsulated by epoxy (10.4, 22.0, and 39.0 μm thick) on PET substrate and in the neutral mechanical configuration of frame (a), in a bent state (R ~ 7.3 mm).

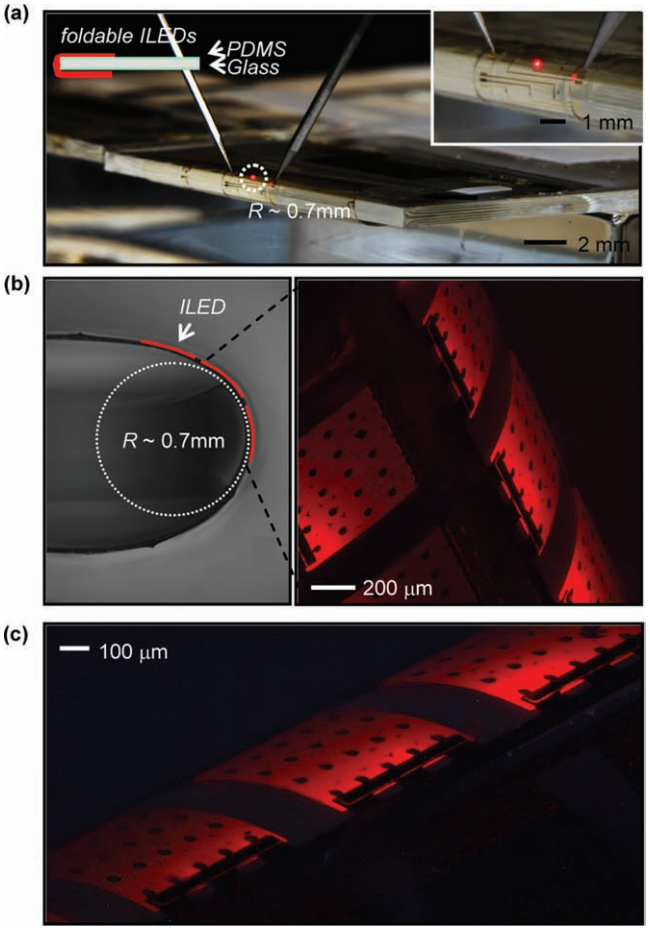

Figure 5. a) Optical images of ILEDs (100 × 100 μm) in a neutral mechanical plane layout, during operation wrapped around the edge of a) a slide glass (1 mm thick). The bending radius is ~0.7 mm. b) Cross sectional optical image of a similar ILED system and composite magnified view to show bending in the individual devices. c) Similar composite image collected at a different viewing angle.

of sheet is ~17 μm which includes the ILEDs, the epoxy interlayer, the metal electrodes and the polyurethane layers. In this configuration, the system can be bent to sharp folds, with R as small as 0.7 mm, with associated wavelength shifts of ~1 nm, close to the resolution limit of our spectrometer (~0.5 nm) and simple means for evaluating the shifts as shown in Figure 4b. Figure 4c describes the calculated maximum strain in the quantum well of the ILED for the previously described encapsulated scheme on PET and the neutral mechanical plane design as a function of bending radius. The labels *a*, *b*, *c*, and *d* correspond to PET, polyurethane, epoxy, and ILED, respectively, in the schematic cross sectional views that appear as insets in Figure 4c. The maximum strain in the quantum well of the ILED decreases as the top encapsulation layer increases for the devices on PET. In nearly neutral mechanical plane designs, the maximum strain in the quantum well dramatically decreases as top polyurethane and epoxy layers match the mechanical effects of the bottom polyurethane layer. Figure 4d shows the dependence of the shift in emission wavelength on the bending strain at several different encapsulation layer thicknesses. The shifts dramatically decrease as the ILED moves toward the neutral mechanical plane. This design provides extreme levels of bendability, as shown in **Figure 5a** for the case of an ILED (100 × 100 μm) wrapped around the edge of a slide glass (thickness ~1 mm), respectively. The left frame in Figure 5b shows a cross sectional optical micrograph; the bending radius is approximately 0.7 mm. For this case, relatively large size ILEDs (500 × 500 μm) were used, for ease of viewing. The curved lines (red) indicate of the approximate locations of the devices. The right frame in Figure 5b shows a composite optical image, formed using images captured at different focal depths, of a 3 × 3 square array of ILEDs. Figure 5c provides a slightly different view of a similar array. In both images, bending of the ILEDs themselves can be clearly observed.

The ideas presented here provide routes to flexible ILEDs with the capacity for bending to small radii of curvature. Careful analysis of the emission properties together with calculations of the bending mechanics and strain induced shifts in the bandgap give insights into the underlying physics and mechanics aspects. The results provide guidelines for the design of light sources with extreme levels of flexibility.

Experimental Section

Fabrication of ILED Devices on Plastic Substrates: The fabrication begins with transfer printing of ILEDs (~2.5 μm thick) formed by

specialized epitaxial semiconductor layers grown on top of a sacrificial layer ($Al_{0.96}Ga_{0.04}As$) on a GaAs wafer. The receiving substrate consists of a sheet of polyethylene terepthalate (PET; Grafix DURA-LAR, 50 μm thick) coated with a thin adhesive layer, as reported in detail elsewhere.[3] The n-contact region of the ILED is defined by exposure of n-GaAs layer through wet etching through the top layers (p-GaAs/p-spreader by $H_3PO_4/H_2O_2/H_2O$ (1:13:12), InAlGaP-based layers by HCl/H_2O (2:1), and n-spreader by $H_3PO_4/H_2O_2/H_2O$ (1:13:12)) of the stacks. An epoxy (SU8-2, Microchem.) as an interlayer protects the sidewalls to prevent electrical shorting and it also planarizes the devices. This material is spin-coated (1500 rpm, 30 sec), cured (65°C for 60 sec and 95°C for 105 sec), lithographically patterned (exposed to UV light at 10 $mWcm^{-2}$ for 10 sec, baked at 95°C for 105 sec, and developed using SU8 developer (Microchem.)) to define contact holes, and then postbaked at 150°C for 20 min to induce cross-linking. A bilayer of Ti/Au (thickness = 20/350 nm), deposited by electron beam evaporation and patterned by photolithography and wet etching, provides (unoptimized) electric contacts with p- and n-GaAs. The ILED devices with metal electrodes are encapsulated by another layer of epoxy (SU8). Multiple thicknesses of this material are achieved using different formulations (SU8-2 and SU8-5, Microchem., spun at 3000 rpm/30 sec) and multiple cycles of spin coating and patterning.

Measurement of Emission Wavelength with Bending: We measured the emission spectra under bending using a high resolution spectrometer (Ocean Optics, HR-4000) and a multimode optical fiber (Thorlabs, 400 μm diameter core). The spectrometer has a resolution of ~0.5 nm, based on a HC-1 grating (200 ~ 1100 nm) and 5 μm slit width. The data points are reported in intervals of ~0.27 nm. The ILED devices on plastic (PET, 50 μm thick) are wrapped on test tubes with different bending radii of 7.3, 4.9, and 3.5 mm. Extremely small radii of curvature (~0.7 mm) are achieved by wrapping the devices on the sharp edge of a glass slide (~1 mm thick) coated with a thin layer of PDMS (~10 μm thick).

Fabrication of ILED Devices Placed in Nearly Neutral Mechanical Plane: A photocurable polyurethane (NOA61) is spin-coated (3000 rpm/60 sec), cured by UV exposure for 1 h on a temporary substrate of PET. The fabrication of ILED devices follows the processing steps described elsewhere. Except for metal probing, the devices formed in this way are encapsulated by the polyurethane and lie near the mechanical neutral plane after removing the PET.

Acknowledgements

We thank T. Banks for help with processing using facilities at the Frederick Seitz Materials Research Laboratory and I.S. Chun for useful discussion. This material is based upon work supported by the National Science Foundation under grant DMI-0328162 and the U.S. Department of Energy, Division of Materials Sciences under Award No. DE-FG02-07ER46471, through the Materials Research Laboratory and Center for Microanalysis of Materials (DE-FG02-07ER46453) at the University of Illinois at Urbana-Champaign. S.-I. Park would like to thank Samsung for doctoral fellowships.

Received: February 16, 2010
Revised: March 6, 2010
Published online: May 14, 2010

[1] S.-C. Lo, P. L. Burn, *Chem. Rev.* **2007**, *107*, 1097.
[2] F. So, J. Kido, P. Burrows, *MRS Bull.* **2008**, *33*, 663.
[3] S.-I. Park, Y. Xiong, R.-H. Kim, P. Elvikis, M. Meitl, D.-H. Kim, J. Wu, J. Yoon, C.-J. Yu, Z. Liu, Y. Huang, K.-c. Hwang, P. Ferreira, X. Li, K. Choquette, J. A. Rogers, *Science* **2009**, *325*, 977.
[4] D. A. Gaul, W. S. Rees, Jr., *Adv. Mater.* **2000**, *12*, 935.
[5] S. Nakamura, G. Fasol, *The Blue Laser Diode: GaN Based Light Emitters and Lasers*, Springer, New York, **1997**.
[6] D.-H. Kim, J.-H. Ahn, W. M. Choi, H.-S. Kim, T.-H. Kim, J. Song, Y. Y. Huang, Z. Liu, C. Lu, J. A. Rogers, *Science* **2008**, *320*, 507.
[7] J. Yoon, A. J. Baca, S.-I. Park, P. Elvikis, J. B. Geddes III, L. Li, R. H. Kim, J. Xiao, S. Wang, T.-H. Kim, M. J. Motala, B. Y. Ahn, E. B. Duoss, J. A. Lewis, R. G. Nuzzo, P. M. Ferreira, Y. Huang, A. Rockett, J. A. Rogers, *Nat. Mater.* **2008**, *7*, 907.
[8] Y.-H. Cheng, C.-M. Chen, C.-H. Cheng, M.-C. M. Lee, *Jpn. J. Appl. Phys.* **2009**, *48*, 021502.
[9] H. Cho, C. Yun, J.-W. Park, S. Yoo, *Org. Electron.* **2009**, *10*, 1163.
[10] J.-W. Kang, W.-I. Jeong, J.-J. Kim, H.-K. Kim, D.-G. Kim, G.-H. Lee, *J. Electrochem. Soc.* **2007**, *10*, J75.
[11] S. Kim, K. Kim, K. Hong, J.-L. Lee, *J. Electrochem. Soc.* **2009**, *156*, J253.
[12] M. A. Meitl, Z.-T. Zhu, V. Kumar, K. J. Lee, X. Feng, Y. Y. Huang, I. Adesida, R. G. Nuzzo, J. A. Rogers, *Nat. Mater.* **2006**, *5*, 33.
[13] D. Y. Khang, H. Jiang, Y. Huang, J. A. Rogers, *Science* **2006**, *311*, 208.
[14] D.-H. Kim, J. Song, W. M. Choi, H.-S. Kim, R.-H. Kim, Z. Liu, Y. Y. Huang, K.-C. Hwang, Y.-w. Zhang, J. A. Rogers, *Proc. Natl. Acad. Sci. USA* **2008**, *105*, 18675.
[15] S. Timoshenko, *Theory of plates and shells*, McGraw-Hill, New York, **1940**.
[16] F. H. Pollak, *Surf. Sci.* **1973**, *37*, 863.
[17] M. Chandrasekhar, F. H. Pollak, *Phys. Rev. B* **1977**, *15*, 2127.
[18] S. H. Pan, H. Shen, Z. Hang, F. H. Pollak, W. Zhuang, Q. Xu, A. P. Roth, R. A. Masut, C. Lacelle, D. Morris, *Phys. Rev. B* **1988**, *38*, 3375.
[19] D. P. Bour, R. S. Geels, D. W. Treat, T. L. Paoli, F. Ponce, R. L. Thornton, B. S. Krusor, R. D. Bringans, D. F. Welch, *IEEE J. Quantum Electron.* **1994**, *30*, 593.